East European Journal of Physics. 2. 398-406 (2024)
DOI:10.26565/2312-4334-2024-2-51 ISSN 2312-4334

IMPLICATIONS OF THE PRESENCE OF Y AS A REACTIVE ELEMENT IN CATHODIC VACUUM ARC TiAlN PROTECTIVE COATING FOR TRIBOLOGICAL APPLICATIONS

O.V. Maksakova[a,b], V.M. Beresnev[a], S.V. Lytovchenko[a]*, M. Čaplovičova[b], L. Čaplovič[b], M. Kusý[b], I.V. Doshchechkina[c]

[a] *V.N. Karazin Kharkiv National University, 4, Svoboby Sq., 61000 Kharkiv, Ukraine*
[b] *Institute of Materials Science, Slovak University of Technology in Bratislava, 25, Jána Bottu Str., 917 24 Trnava, Slovakia*
[c] *Kharkiv National Automobile and Highway University, 25, Ya. Mudryi St., 61200 Kharkiv, Ukraine*
**Corresponding Author e-mail: s.lytovchenko@karazin.ua*
Received April 4, 2024; revised May 11, 2024; accepted May 19, 2024

The results of studies of the influence of Y as a reactive element on the properties of TiAlN coatings obtained by the method of vacuum-arc deposition are given. Changes in the structure and properties were analyzed using SEM in combination with EDX, XRD, indentation analysis and wear analysis. It is shown that the presence of Y changes the crystalline phase of the $Ti_{0.6}Al_{0.34}Y_{0.06}N$ coating. It consists of a combination of a cubic NaCl structure (basic phase) and a wurtzite structure (additional phase). In addition, it leads to a small grain size (12 nm) and a nano-columnar structure. The high hardness is partly the result of solution hardening due to the inclusion of larger Y atoms in the TiAlN lattice at the locations of the metal atoms. The reduced grain size of 12 nm also helps to increase the hardness of the coating. The hardness is 31 ± 2.5 GPa, the modulus of elasticity is 394.8 ± 35.8 GPa. The residual stress is approximately three times (−3352 ± 64 MPa) higher than the TiAlN coating (−720 MPa). In addition, a high level of compressive stress contributes to an increase in hardness, since defects responsible for their own compressive stress are an obstacle to dislocation movement. The improved hardness of the experimental coating can be explained by a triple effect: solution strengthening, grain grinding and high residual compressive stress. The addition of Y indicates a slower growth of the oxide layer on the surface of the coating during the wear test. After the addition of Y, Y ions preferentially separate at the grain boundaries and therefore effectively delay the inward diffusion of oxygen. The addition of Y promotes the formation of dense Al_2O_3, which is effective in restraining diffusion and therefore protects the coating from oxidative wear.
Keywords: *Vacuum arc deposition; Coatings; Wurtzite phase; Hardness; Wear; Critical loads*
PACS: 61.46.-w; 62.20.Qp; 62-25.-g; 81.15.Cd

INTRODUCTION

The machining industry demands high-performance cutting tools to handle the cutting of new, difficult-to-cut materials. Although tooling does not exceed 5 % of the total manufacturing costs, it has a significant impact on productivity since the tool's capability influences the efficiency of the manufacturing process [1, 2]. Cutting speed is an essential factor in machining, which greatly affects the production cost per part and reduces it by increasing the number of parts produced at a given time. Stainless steels are considered the most difficult-to-cut materials due to their specific properties such as high toughness, work-hardening, and low heat conductivity [3]. This makes it difficult to produce high-quality machined surfaces and dramatically increases the production cost. To meet the ever-increasing demand for higher productivity levels, the cutting speed is conventionally increased, which results in the tool operating under severe service conditions, significantly affecting its life [4]. Therefore, it is crucial to develop new tools with advanced coatings that can withstand these high-speed and high-temperature conditions in the cutting zone.

The conventional advantages of applying protective coatings on cutting tools are assigned to improving wear resistance, heat resistance, corrosion resistance, strength, toughness, and tool life [5, 6]. The practice of coating cutting tools for machining steels initially used binary coatings like TiN and CrN [7, 8]. It is a fact that the use of binary nitride coatings (i.e. TiN or CrN) is limited at elevated temperatures exceeding 500 °C). However, for modern high-speed machining, thermal-mechanical stability is an absolute necessity at temperatures reaching and surpassing 1000 °C [9].

The conjunction of the outstanding mechanical properties of binary metal nitrides (BMNs) and enhanced oxidation resistance caused by the formation of dense, chemically stable Al-rich oxide layer on the surface of coatings, make the metastable solid solution TiAlN coatings widely applied in machining stainless steel [10, 11]. Significant upgrading of mechanical and thermal properties and machining performance are the major benefits of the Al incorporation into the TiN lattice. However, Al content must be strictly controlled. Below an Al content of 67 at. %, a single-phase crystal structure forms by substitution of Ti by Al in a fcc-TiN lattice, which typically yields the highest hardness and elastic modulus [12]. Above ~67 at % of Al, the coating properties start to retrogress due to the formation of mixed NaCl-cubic and hcp structures (wurtzite phase) [13]. Based on the available reports, the TiAlN coatings can function effectively up to temperatures between 750 – 950 °C. Rogstrom et al. [14] observed that above 930 °C, wurtzite-AlN transformation occurs, resulting in a loss of properties and functionality of TiAlN coatings. Chen et al. [15] and Grossmann et al. [16] also reported temperatures of 950 °C and 980 °C, respectively, as critical for $Ti_{1-x}Al_xN$ ($0.4 \leq x \leq 0.75$) coatings.

Cite as: O.V. Maksakova, V.M. Beresnev, S.V. Lytovchenko, M. Caplovicova, L. Čaplovič, M. Kusýb, I.V. Doshchechkina, East Eur. J. Phys. 2, 398 (2024), https://doi.org/10.26565/2312-4334-2024-2-51

According to Mayrhofer et al. [11], the fcc- $Ti_{1-x}Al_xN$ coatings exhibit adaptive behavior during annealing resulting in increased hardness. This property is beneficial in applications that involve frictional heating during machining. Studies [17, 18] have shown that temperatures can rise up to 1000 °C in the cutting zone during high-speed machining of difficult-to-cut materials. Further improvement is necessary to maintain desired productivity levels when machining under severe tribological conditions.

One effective approach to customize the characteristics of TiAlN coating is to incorporate alloying elements that possess high melting points, thermal conductivity, and a tendency to form dense oxide layers [19]. For instance, the addition of V induces an enhanced wear performance at high temperatures owing to the formation of lubricious phase oxides V_2O_5 with a self-lubricating effect. In addition, coatings demonstrate superb oxidation resistance due to the presence of an Al-rich oxide top layer, as supported by various studies [20, 21]. For TiAlSiN coatings, excellent mechanical and thermal properties are assured by the Si-existence of solution and/or amorphous a-SiN_x tissue phase and depend on the deposition parameters and the Si content [22, 23]. The incorporation of Nb and Zr also has a beneficial effect on the TiAlN coatings on the mechanical and thermal properties [24, 25]. The influence of Mo addition to TiAlN-based coatings is positively assessed in [26, 27]. Depending on differing Mo contents (7.7 – 12.1 at. %) coatings demonstrate the improvement of mechanical properties, particularly wear behavior and resistance to pitting corrosion. The structural and morphological evolution of arc-evaporated TiAlWN coatings obtained at different bias voltages is studied in the work [28]. The addition of W positively influences morphology concerning macroparticle incorporation as well as surface roughness. The coatings exhibit advanced ductility and stiffness, as evidenced by the significantly high H^3/E^2 ratios. Another element that can be used as a doping element to TiAlN is Yttrium. Several studies [29 – 31] have pointed out that incorporating Y to $Ti_{1-x}Al_xN$ thin films can be a promising approach to improve the corrosion and oxidation resistance combined with maintaining hardness and elasticity at high temperatures. Its high melting point, electronic configuration, and large atomic radius influence the formation of the cubic nitride and hence the age-hardening effect of $Ti_{1-x-y}Al_xY_yN$. According to a study by Rachbauer et al. [32], the process of age hardening in $Ti_{1-x-y}Al_xY_yN$ is not only affected by the increase in strain due to lattice mismatch but also depends on the bindings present. Aninat et al. [33] reported that the addition of Y to the TiAlN resulted in better mechanical properties and increased hardness. However, it reduced the compressive stress. Moser et al. [34] investigated the thermal stability of $Ti_{1-x}Al_xN$ coating with Y addition through the DC magnetron sputtering process. It was found that after annealing at high temperatures, there was an increase in hardness. Donohue et al. [35] found that a low concentration yttrium substitution into the metastable Ti_xAl_yCrYN coatings significantly refines the grain. The $Ti_{0.43}Al_{0.52}Cr_{0.03}Y_{0.02}N$ demonstrate considerably improved oxidation and corrosion resistance compared to $Ti_{0.44}Al_{0.53}Cr_{0.03}N$ coatings. Yttrium shows a high tendency to form an oxide along the grain boundaries and as well at the metal-oxide interface. On the metal-oxide interface, Y inhibits the formation of voids and promotes the creation and adhesion of a dense protective oxide layer (Y_2O_3). On the other hand, at the grain boundaries, it functions as a barrier to fast diffusion paths within the oxide scale [36]. In simple terms, yttrium acts like a 'plug' that stops the inward diffusion of oxygen and the outward diffusion of metal components of the coating. This is especially true for diffusion along grain boundaries and surfaces [35]. However, as the Y content increases from 3 to 9 at. %, a change in the structure occurs. A single-phase cubic solid solution crystal structure converts to a mixed cubic and wurtzite structure (at 5 at. % of Y), and finally to a single-phase wurtzite structure at 9 at. % of Y [32, 34].

The present study aimed to identify and explore experimentally, the structure, composition, and properties of arc-evaporated TiAlYN coating with 5 at. % of Y in a target for understanding the protective perspectives of this type of coating and suggesting its working conditions.

Before describing the experimental details and discussing the obtained results, we want to briefly explain the benefits of alloying elements, including Yttrium, to TiAlN coatings from the recently published first-principles study [37]. The summarizing of these data contributes to a better atomic-scale understanding of TiAlN coatings alloyed with the fourth element for their potential applications.

FIRST-PRINCIPLES STUDY REVIEW

By using first-principles calculations, eight elements (La, Ce, Y, Hf, Zr, Ta, Cr, Si) were doped on the $Ti_{0.5}Al_{0.5}N$ (001) surface to comparatively study the effect of different doping atoms. All computational details can be found in [37].

To determine the doping of X atom on the surface, the formation energy of X replacing one metal (Al and Ti) or non-metal (N) atom on the $Ti_{0.5}Al_{0.5}N$ (001) surface layer was calculated. The formation energies of X substituting the Al atoms on the $Ti_{0.5}Al_{0.5}N$ (001) surface are the following: −1.160 eV (La), −1.119 eV (Ce), −1.336 eV (Y), -1.258 eV (Hf), −0.913 eV (Zr), 0.497eV (Ta), 1.586 eV (Cr), 1.785 eV (Si). The surface configuration of Al substituted by X atom in TiAlN is shown in Fig. 1.

Based on calculated results, it can be realized that the formation energies of La, Ce, Y, Hf, and Zr replacing the Al atom on the $Ti_{0.5}Al_{0.5}N$ (001) surface are negative, in comparison to the atoms of Ta, Cr, and Si. This implies that for La, Ce, Y, Hf, and Zr doping, the structures are expected to be synthesized easily in experiments due to lower formation energy. Among these five doped elements, Y is more inclined to replace the surface Al atom due to its lowest formation energy of −1.336 eV.

The adsorption behavior of oxygen on the $Ti_{0.5}Al_{0.5}N$ (001) surface with the addition of Y atoms has been analyzed along with formation energy. These findings can be especially useful when studying the tribological behavior of TiAlN-based coatings, particularly in relation to wear mechanisms that can help identify potential areas of application.

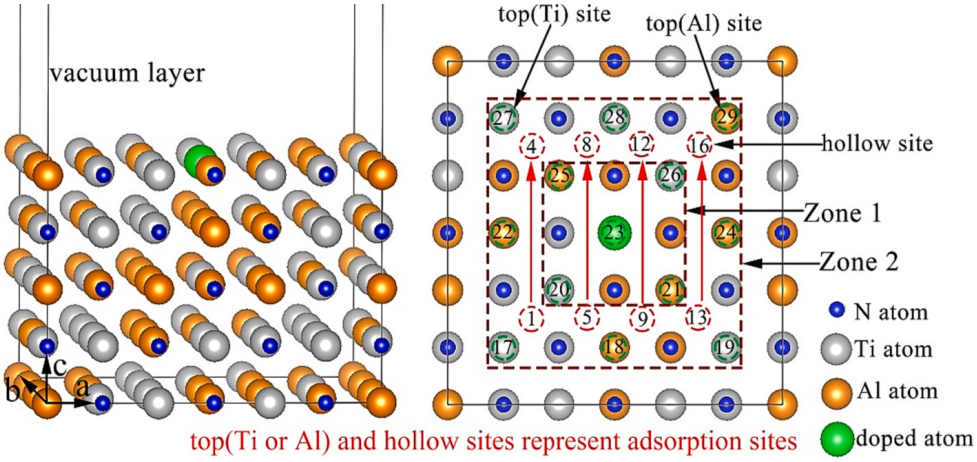

Figure 1. The surface slab (left panel) and surface adsorption sites (right panel) of $Ti_{0.5}Al_{0.5}N$ (001) surface with X-doped. In the figure, Zone 1 is included in Zone 2. Adopted from [37].

Fig. 2 illustrates the bonding behavior between an Oxygen atom and $Ti_{0.5}Al_{0.5}N$ (001) surface without and with a doped Y atom. When comparing the $Ti_{0.5}Al_{0.5}N$ (001) surface to the Y-doped surface, it was found that the Y-doped surface has a stronger attraction to O atoms. This was observed by examining the structures of oxygen atoms adsorbed at twenty-nine adsorption sites. It was discovered that the Y atom can chemically bond with O atoms from its surrounding area, indicating that Y has a high affinity for O.

In Fig. 2b, except for the 8, 9, 10, and 11 sites, the other O atoms with different adsorption sites are attracted by the Y atom, eventually forming chemical bonds. Oxygen atoms located at adsorption sites 1, 5, 6, and 7 migrate to the green circle position in the lower left corner due to the attraction of the Y atom, forming the Y-O-Ti bond. On the other hand, when O atoms are located at sites 3 and 4 (top (Al)), they shift to the green circle positions in the upper left and lower right corners respectively, forming the Y-O-Al bond. Finally, when O atoms are at sites 2 and 12, they are attracted by the Y atom to the green circle position in the upper right corner, forming the Y-O-Ti bond.

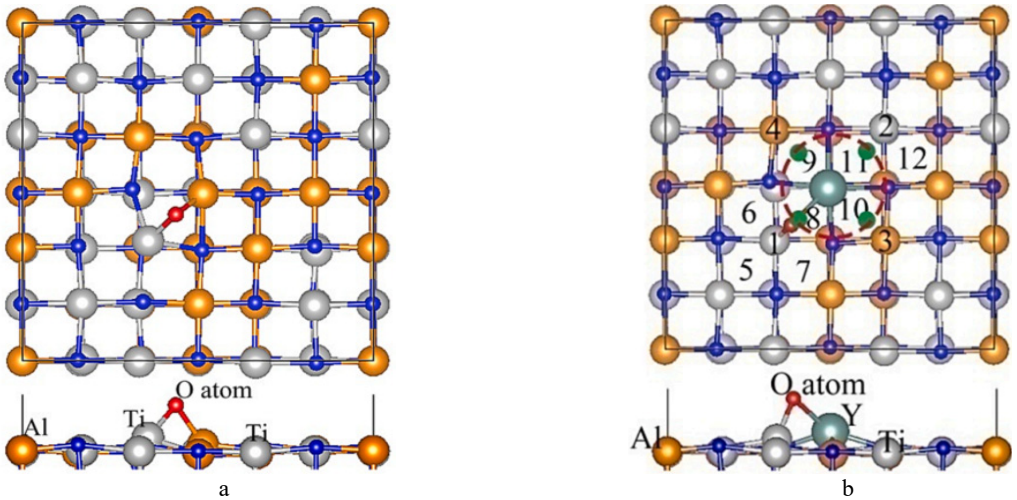

Figure 2. The adsorption configuration of $Ti_{0.5}Al_{0.5}N$ (001) surface without and with Y doped. Adopted from [37].

Therefore, the analysis of bond characteristics between O and Y atoms on the $Ti_{0.5}Al_{0.5}N$ (001) surface suggests that when Y atoms substitute Al atoms on the surface, they tend to form hybrid oxides (X-O-Al or X-O-Ti) in the initial stage of oxidation, rather than simple self-metal oxides (X-O). This conclusion is supported by experimental results that show the oxidation products include complex oxides such as $Y_2Ti_2O_7$ [38] and $YAlO_3$ [39]. It is noteworthy that $Y_2Ti_2O_7$ has a higher hardness of 12.1 GPa compared to Y_2O_3 (6.9 – 9.1 GPa) and TiO_2 (11 GPa). However, Young's modulus of $Y_2Ti_2O_7$ (262 GPa) is similar to that of TiO_2 (266 – 270 GPa) and 25% higher than that of Y_2O_3 (188 GPa) [40].

In summary, the results of the first-principal study show that TiAlYN coatings are interesting as protective materials able to work successfully in tribological conditions due to the modification of the surface structure resulting from oxide transformations.

EXPERIMENTAL DETAILS

Deposition

TiAlYN coatings were deposited by the cathodic arc evaporation method in a non-commercial coating machine. AISI steel square bars of dimension 20mm×20mm×2 mm were chosen as the substrates since these are some of the most widely used cutting tool materials in the machining industry. $Ti_{0.5}Al_{0.45}Y_{0.05}$ alloys were utilized as the cathode materials, which were manufactured by the powder metallurgy technique. Prior to the deposition, substrates were ultrasonically cleaned. Then they were mounted to a rotating substrate carousel. The chamber was pumped to a base vacuum lower than 4×10^{-3} Pa. All targets were pre-sputtered for 7 min to remove the surface contaminants. The substrates were plasma etched in an argon atmosphere (0.2 Pa) for 10 min. Plasma etching removes surface contaminants and creates fresh surfaces for the nucleation and growth of coatings. Coatings' deposition was carried out in a nitrogen environment at a nitrogen pressure (P_N) of 0.53 Pa and a negative bias applied to the substrate (U_b) of 200 V. During the deposition process, the temperature on substrates was about 450 °C, and deposition time lasted 60 min.

Characterization

The cross-sectional microstructure at different magnifications, as well as morphology of the surface after wear tests were studied using scanning electron microscopy in a Quanta 600 FEG and FEI Nova NanoSEM 450 microscopes. The phase state was characterized using X-ray diffraction in a Panalytical Empyrean X-ray diffractometer in Co-Kα radiation (λ = 0.1789 nm). Identification of the phases and calculation of main crystal structural parameters was done using Malvern Panalytical's XRD software.

The microhardness was measured using an automated Anton Paar NHT ultra microhardness tester equipped with a diamond Berkovich tip. The maximum applied load was 10 mN and the loading time was 20 s. During the test, the indentation depth was controlled within 10 % of the coating thickness to avoid the effect of the substrate.

The scratch test was performed in a Bruker UMT-2 tester under the minimal load of 0.2 N and the maximal load of 46 N. The size of the scratch was 5 mm.

Ball-on-disc tribotest was carried out in a Bruker UMT-2 tester. The counterball was 6.3 mm WC-Co. The applied load was 5 H, the sliding speed was 200 rpm, and the sliding time was 30 min.

RESULTS

Fig. 3 shows the surface and cross-sectional SEM micrographs and corresponding EDX elemental mapping of TiAlYN coating. It notes that the surface of the coating has ample macroparticle fraction and inapparent facet morphology. Macroparticles are usually present when deposition takes place with the PVD method, and they lead to surface irregularities. The fractured cross-section image of the coating reveals that the coating is well-grown and adherent to the steel substrate. The coating exhibits a nano-columnar microstructure.

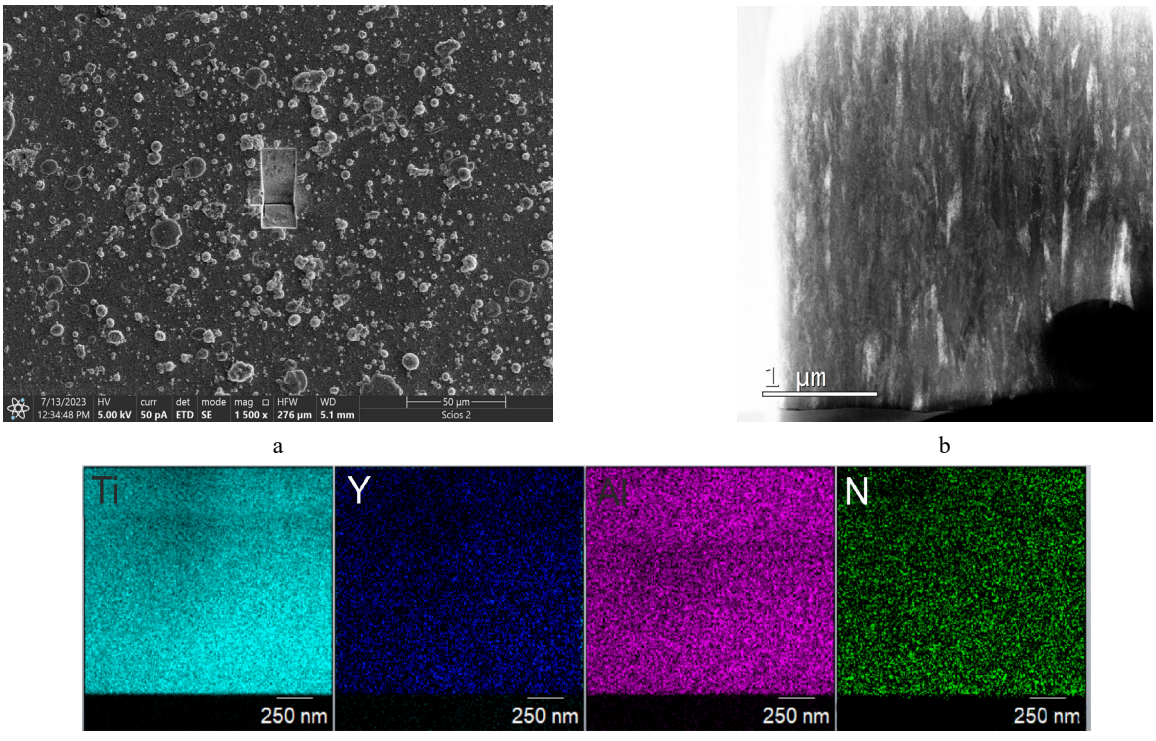

a b c

Figure 3. SEM micrographs of TiAlYN coating in planar (a) and cross-section (b) views and corresponding EDX elemental mapping (c).

The elemental composition of the coating was determined by EDX mapping in the SEM. The result shows that the distributions of all constituent elements in the coating are quite uniform. The chemical composition of the coating is the following: $Ti_{0.6}Al_{0.34}Y_{0.06}N$. Since the nitrogen pressure used for the deposition was 0.53 Pa, the coating composition is stoichiometric. The Al concentration in the coating is lower than that of the target composition, while the amount of Ti and Y in the coating is higher compared to the target. This can be explained by the large difference in the atomic mass of the metallic components, due to which the rate of scattering in the gas phase for Al is higher and more Al re-sputters during coating growth.

XRD pattern of the coating is shown in Fig. 4. The 2θ peak positions for standardized c-TiN (a_c = 4.24 Å, ref. code 03-065-0414), c-AlN (a_c = 4.12 Å, (ref. code 00-046-1200) and c-$Al_{0.5}Ti_{0.5}N$ (a_c = 4.19 Å, ref. code 01-071-5864), c-YN (a_c = 4.87 Å, ref. code 01-071-9847), h-Ti_2AlN (a_h = 2.98 Å, c_h = 13.61 Å, c_h/a_h = 4.56, ref. code 00-055-0434) and h-AlN (a_h = 3.11 Å, c_h = 4.98 Å, c_h/a_h = 1.60, ref. core 01-086-4277) are labeled with different colors and symbols.

The coating exhibits strong {200} preferred orientation. It can be seen from the pattern, the Y prefers to dissolve into the AlTiN-forming solid solution rather than segregating as a second YN phase (formation of separate peaks) [41]. The dissolution of the Y into the AlTiN lattice produces an increased lattice parameter of the TiAlYN coating. This is due to Y having a larger atomic radius compared to those of the Ti and Al. Additionally, a broadening of the characteristic peaks of the solid solution TiAlYN can be observed after the Y addition, which can be attributed to the grain refinement. The average grain size of the coating is 12 nm.

As the Ti content in the coating is quite high, the cubic peaks at the XRD pattern shift towards higher angles. Moreover, the presence of Y results in the formation of an extra wurtzite phase, which is evident in the diffraction pattern at 38.5° and 46.8° diffraction angles. This indicates that the coating has a significant amount of the wurtzite phase. These results correspond well with other literature reports [30, 32] and ab initio findings, which suggest that at high Y content, the solubility of Al in the cubic single phase field decreases.

The main mechanical and tribological properties of TiAlYN coating as well as thickness are summarized in Table 1. The formation of the wurtzite phase due to high Y and Al content, as mentioned above, can result in decreased hardness values as compared to the coatings with a metastable single phase (cubic solid solution). For the experimental coating, the value of hardness is 31 ± 2.5 GPa which is comparable to the hardness for the single-phase cubic coatings, which vary between 30 and 35 GPa [34]. Such high hardness can be explained by solid solution strengthening and the induced microstrain due to the incorporation of Y atoms. With increasing Y content, the octahedrally coordinated sp^3d^2 hybridisation is weakened and the tetrahedral sp^3 hybridisation is favoured resulting in a promotion of the wurtzite structure [32].

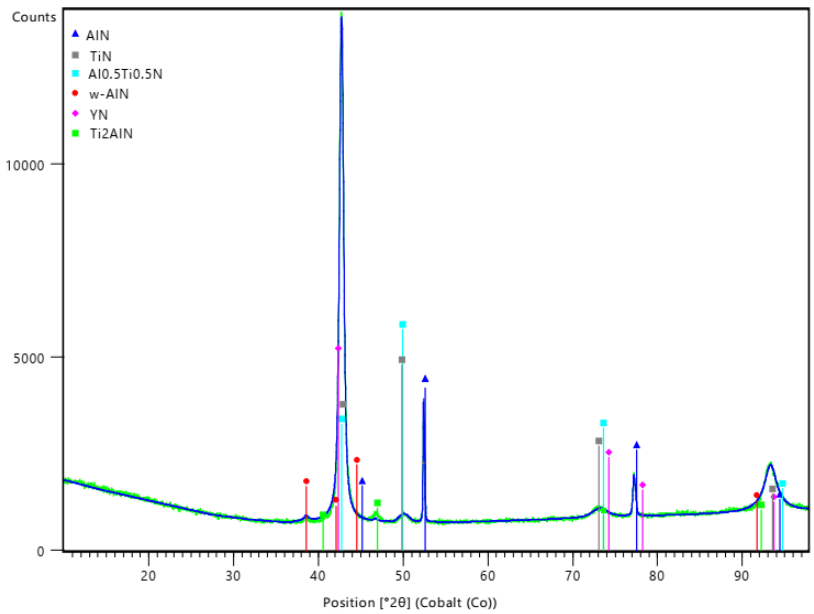

Figure 4. Diffraction pattern of TiAlYN coating

It is generally accepted that higher residual stresses lead to higher hardness and that high residual compressive stresses are conducive to higher fracture toughness [37]. It is clear that the residual stress of experimental coating is −3352 ± 64 MPa, this high value ensures the high hardness. Table 1 contains two other hard mode ratios, such as H/E and H^3/E^2, which are also accurate and reliable measures of wear resistance. H/E correlates with elastic strain failure capacity, with a larger ratio implying a higher fracture toughness of the coating, while a large H^3/E^2 is a strong indication of wear resistance, plastic deformation resistance, and fracture resistance. As one can see, the values of H/E and H^3/E^2 are respectively = 0.078 ± 0.07 and 0.191 ± 0.011. This means that coating has less tensile stress in the tensile stress concentration zone and, therefore, is less prone to cracking as well as has high fracture toughness. The friction

coefficient of the coating is around 0.6 – 0.65. The running-in stage of the coating was 450 s, and then the fluctuations in the friction curve stopped.

Table 1. Functional properties of TiAlYN coating

	Value
Thickness Δ, micron	6.5
Hardness H, GPa	31 ± 2.5
Elastic modulus E, GPa	394.8 ± 35.8
Elastic strain to failure H/E	0.078 ± 0.007
Resistance to plastic deformation H^3/E^2	0.191 ± 0.011
Residual stress, MPa	−3352 ± 64
Friction coefficient	0.6-0.65
Load of buckling cracks Lc_1, N	8.5 ± 1.5
Load of buckling spallation Lc_2, N	26.7 ± 1.8

Coating adhesion is an important property that may significantly affect coating performance, especially when adhesion wear is present. Coating failure is usually divided into two stages: first, the initial exposure of the substrate, where cohesion failure occurs inside the coating, corresponding to Lc_1; and then the complete spalling of the coating from the substrate, that is, interfacial damage or adhesion failure, corresponding to Lc_2 [42]. It has been determined that the adhesion strength of the experimental coating is 26.7 ± 1.8 N. The smaller the grains in the steel substrate, the more coherent or semi-coherent interface becomes between the substrate and the coating, leading to greater coating adhesion.

Fig. 5 shows the SEM image of the morphology of TiAlYN coating after a complete wear test and the corresponding EDX graph of chemical composition. Wear failure inside the groove is characterized by flaky chipping [42], without any substrate exposure. In addition, adhesion as well as furrows can be observed inside the wear track. The edges of the wear track show some accumulation of abrasive debris, and the EDS results show a large amount of Fe, C, and O elements, which is evidence of adhesive wear. It is worth mentioning that experimental coating has relatively high roughness caused by macroparticle fraction, the hard protrusions and defects on the coating surface fall off during friction and participate in the frictional behavior of the coating and the ball as abrasive particles, so that the wear pattern contains a number of grooves. As a result, three-body friction occurs, which reduces the contact between the coating and the ball, thus reducing the friction coefficient and wear rate.

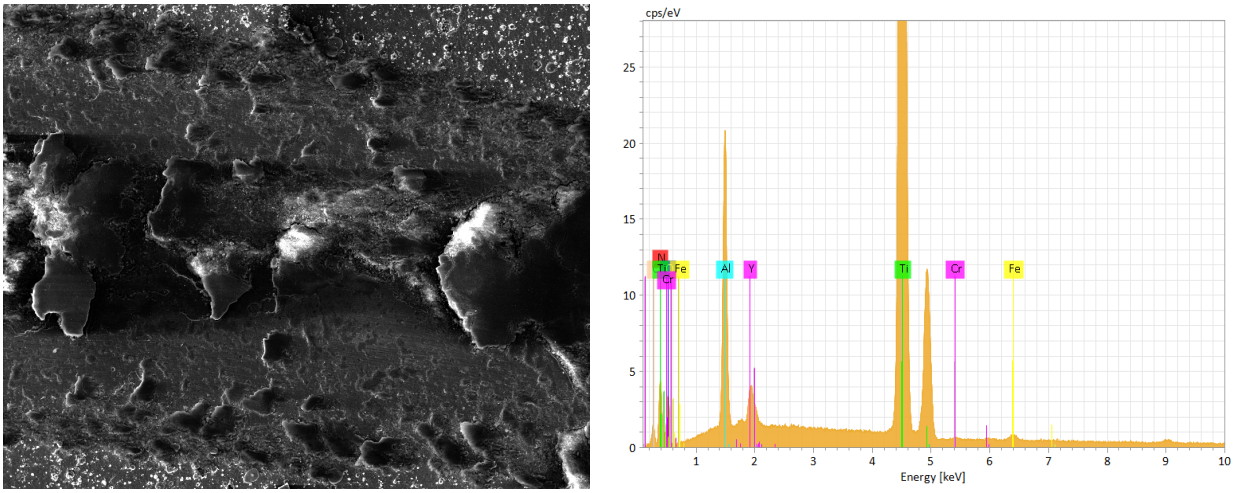

Figure 5. Image of the wear track on the surface (left) and corresponding EDX elemental graph (right) of TiAlYN coating.

In addition, the high wear performance of the coatings is also due to the high elastic modulus of 394.8 ± 35.8 GPa. During the wear test, the elastic strain energy stored in the coating increased as the pressure at the wear groove increased. Until the strain energy increased, until it directly broke the coating structure, and no significant coating fragmentation was produced.

DISCUSSION

The fact that experimental coating is composed of mixed phase structure (cubic NaCl-type and hexagonal wurtzite-type) demonstrates that the crystalline phase of the coating is affected by the addition of 5 at. % Y. Thus, the addition of large and therefore relatively immobile Y atoms (atomic radius 0.18 nm) leads to continuous re-nucleation during deposition [43, 44]. Also, strains due to the addition of Y promote the re-nucleation process. In sum, $Ti_{0.6}Al_{0.34}Y_{0.06}N$ coating exhibits fine grain size (12 nm) and nano-columnar structure.

In comparison with TiAlN coating, the hardness of $Ti_{0.6}Al_{0.34}Y_{0.06}N$ coating is comparatively identical (H = 31 ± 2.5 GPa). The high hardness partly results from the solution hardening due to the incorporation of larger Y

atoms into the TiAlN lattice at the metal atom sites. The reduced grain size of 12 nm also helps to increase the coating hardness. Moreover, the high level of compressive stress contributes to enhanced hardness, since the defects responsible for the compressive intrinsic stress act as the obstacles for dislocation movement [45]. Therefore, the improved hardness of experimental coating can be attributed to triple effects: solution hardening, grain refinement, and high residual compressive stress.

The residual stress of $Ti_{0.6}Al_{0.34}Y_{0.06}N$ coating (−3352 ± 64 MPa) is approximately three times that of TiAlN coating (−720 MPa) [46] and compatible with that of TiAlTaN coating (−3283 ± 92) [47]. Residual stress has a pronounced influence on the properties of coatings. High compressive stress increases the hardness of $Ti_{0.6}Al_{0.34}Y_{0.06}N$ coating. However, it also reduces the adhesion between coating and substrate up to a point where spallation occurs during the adhesive test. Therefore, it is necessary to optimize the residual stress value and improve substrate treatment in the future.

The wear resistance of $Ti_{0.6}Al_{0.34}Y_{0.06}N$ coating is relatively high. The addition of Y suggests the retarded growth of the oxide layer on the coating surface during wear testing. In general, while the wear testing of TiAlN coating, there are transport mechanisms: grain boundary inward transport of oxygen anions and grain boundary outward transport of metal cations. After the Y addition, Y ions are preferentially segregate at the grain boundaries, and therefore effectively retards the inward diffusion of oxygen [48, 49]. Consequently, the growth of the oxide layer is retarded. The retarded growth of the oxide layer also benefits from the formation of oxide phases, such as Y_2O_3 and Al_2O_3. The comparison of Gibbs free energy for the formation of Y_2O_3, Al_2O_3, and TiO_2 shows that Y has the highest affinity for oxygen. The strong interaction between Y and O inevitably inhibits the process of rutile TiO_2 formation. Besides, the first principal study, as well as several experimental investigations, indicate that the addition of Y promotes the formation of dense Al_2O_3, which is effective in restraining diffusion and therefore protects the coating from oxidative wear.

CONCLUSION

In this work, the implications of the presence of Y as a reactive element in cathodic vacuum arc TiAlN protective coating were investigated. The changes in the structure and properties were analyzed using SEM combined with EDX, XRD, indentation, and wear analyses. The following conclusions were obtained:

(1) The addition of Y changes the crystalline phase of $Ti_{0.6}Al_{0.34}Y_{0.06}N$ coating. It consists of a combination of cubic NaCl-type structure (base phase) and wurtzite structure (additional phase). Moreover, it results in fine grain size (12 nm) and nano-columnar structure.

(2) The formation of a w-AlN (wurtzite structure) does not deteriorate the mechanical properties of the coating. The hardness is 31 ± 2.5 GPa and the elastic modulus is 394.8 ± 35.8 GPa. The residual stress is approximately three times (−3352 ± 64 MPa) that of TiAlN coating (−720 MPa). The high mechanical characteristics can be attributed to solution hardening, grain refinement, and high residual compressive stresses.

(3) Abrasive wear and adhesive wear occurred in wear tests of the coating. High macroparticle fracture on the surface reduces the damage from adhesive wear, and, therefore, reduces the coating peeling during friction.

Acknowledgment

The EU NextGenerationEU through the Recovery and Resilience Plan for Slovakia (project nº. 09I03-03-V01-00028) is acknowledged for financial support. The authors were honored to be supported by the Ministry of Education and Science of Ukraine (project nº 0124U001127).

Notes

The authors declare no competing financial interest. The authors declare that they have no known competing financial interests or personal relationships that could have appeared to influence the work reported in this paper.

ORCID

Olga Maksakova, https://orcid.org/0000-0002-0646-6704; **Vyacheslav Beresnev**, https://orcid.org/0000-0002-4623-3243
Serhiy Lytovchenko, https://orcid.org/0000-0002-3292-5468; **Mária Čaplovičová**, https://orcid.org/0000-0003-4767-8823
L'ubomír Čaplovič, https://orcid.org/0000-0002-2280-008X; **Martin Kusý,** https://orcid.org/0000-0002-5553-1680
Irina Doshchechkina, https://orcid.org/0000-0002-6278-7780

REFERENCES

[1] Y. Deng, W. Chen, B. Li, C. Wang, T. Kuang, and Y. Li, "Physical vapor deposition technology for coated cutting tools: a review," Ceram. Int. **46**, 18373–18390 (2020). https://doi.org/10.1016/j.ceramint.2020.04.168

[2] B. Grossmann, A. Jamnig, N. Schalk, C. Czettl, M. Pohler, and C. Mitterer, "Tailoring age hardening of $Ti_{1-x}Al_xN$ by Ta alloying," J. Vac. Sci. Technol. A, **35**(6), 060604 (2017). https://doi.org/10.1116/1.4995000

[3] T. Akasawa, H. Sakurai, M. Nakamura, T. Tanaka, and K. Takano, "Effects of free-cutting additives on the machinability of austenitic stainless steels," J. Mater. Process. Technol. **143–144**(1), 6–71 (2003). https://doi.org/10.1016/S0924-0136(03)00321-2

[4] N. Sharma, K. Gupta, "Influence of coated and uncoated carbide tools on tool wear and surface quality during dry machining of stainless steel 304," Mater. Res. Express, **6**(8), (2019). https://doi.org/10.1088/2053-1591/ab1e59

[5] N. Schalk, M. Tkadletz, and C. Mitterer, "Hard coatings for cutting applications: physical vs. chemical vapor deposition and future challenges for the coatings community," Surf. Coat. Technol. 429 (2022). https://doi.org/10.1016/j.surfcoat.2021.127949

[6] K. Bobzin, "High-performance coatings for cutting tools," CIRP J. Manuf. Sci. Technol. **18**, 1–9 (2017). https://doi.org/10.1016/j.cirpj.2016.11.004

[7] O. Kessler, Th. Herding, F. Hoffmann, and P. Mayr, "Microstructure and wear resistance of CVD TiN-coated and induction surface hardened steels," Surf. Coat. Technol. **182**(2), 184–191 (2004). https://doi.org/10.1016/j.surfcoat.2003.08.054
[8] M.-Y. Wee, Y.-G. Park, and T.-S. Kim, "Surface properties of CrN-coated Ti–6Al–4V alloys by arc-ion plating process," Materials Letters, **59**(8–9), 876–879 (2005). https://doi.org/10.1016/j.matlet.2004.11.035
[9] C. Ducros, and F. Sanchette, "Multilayered and nanolayered hard nitride thin films deposited by cathodic arc evaporation. Part 2: Mechanical properties and cutting performances," Surface and Coatings Technology, **201**(3-4), 1045-1052 (2006). https://doi.org/10.1016/j.surfcoat.2006.01.029
[10] T. Leyendecker, O. Lemmer, S. Esser, and J. Ebberink, "The development of the PVD coating TiAlN as a commercial coating for cutting tools," Surf. Coat. Technol. **48**, 175–178 (1991). https://doi.org/10.1016/0257-8972(91)90142-J
[11] P.H. Mayrhofer, A. Horling, L. Karlsson, J. Sjolen, T. Larsson, C. Mitterer, and L. Hultman, "Self-organized nanostructures in the Ti-Al-N system," Appl. Phys. Lett. **83**, 2049–2051 (2003). https://doi.org/10.1063/1.1608464
[12] M. Bartosik, H.J. Böhm, C. Krywka, Z.L. Zhang, and P.H. Mayrhofer, "Influence of phase transformation on the damage tolerance of Ti-Al-N coatings," Vacuum, **155**, 153–157 (2018). https://doi.org/10.1016/j.vacuum.2018.06.001
[13] L. Chen, J. Paulitsch, Y. Du, and P.H. Mayrhofer, "Thermal stability and oxidation resistance of Ti-Al-N coatings," Surf. Coatings Technol. **206**(11–12), 2954–2960 (2012). https://doi.org/10.1016/j.surfcoat.2011.12.028
[14] L. Rogström, J. Ullbrand, J. Almer, L. Hultman, B. Jansson, and M. Odén, "Strain evolution during spinodal decomposition of TiAlN thin films," Thin Solid Films, **520**(17), 5542–5549 (2012). https://doi.org/10.1016/j.tsf.2012.04.059
[15] L. Chen, J. Paulitsch, Y. Du, and P.H. Mayrhofer, "Thermal stability and oxidation resistance of Ti-Al-N coatings," Surf. Coat. Technol. **206**(11–12), 2954–2960 (2012). https://doi.org/10.1016/j.surfcoat.2011.12.028
[16] B. Grossmann, N. Schalk, C. Czettl, M. Pohler, and C. Mitterer, "Phase composition and thermal stability of arc evaporated $Ti_{1-x}Al_xN$ hard coatings with $0.4 \leq x \leq 0.67$," Surf. Coat. Technol. **309**, 687–693 (2017). https://doi.org/10.1016/j surfcoat.2016.11.015
[17] H. Willmann, P.H. Mayrhofer, P.O. Persson, A.E. Reiter, L. Hultman, and C. Mitterer, "Thermal stability of Al-Cr-N hard coatings," Scr. Mater. **54**(11), 1847–1851 (2006). https://doi.org/10.1016/j.scriptamat.2006.02.023
[18] B. Li, "A review of tool wear estimation using theoretical analysis and numerical simulation technologies," Int. J. Refract. Met. Hard Mater. **35**, 143–151 (2012). https://doi.org/10.1016/j.ijrmhm.2012.05.006
[19] V.F.C. Sousa, F.J.G. Da Silva, G.F. Pinto, A. Baptista, and R. Alexandre, "Characteristics and Wear Mechanisms of TiAlN-Based Coatings for Machining Applications: A Comprehensive Review," Metals, **11**, 260 (2021). https://doi.org/10.3390/met11020260
[20] M. Pfeiler, et al., "On the effect of Ta on improved oxidation resistance of Ti–Al–Ta–N coatings," J. Vac. Sci. Technol. A Vac. Surf. Film. **27**(3), 554–560 (2009). https://doi.org/10.1116/1.3119671
[21] A. Hemmati, M. Abdoos, and S.C. Veldhuis, "Developing Ti-Al-Ta-N based coatings: Thermal stability, oxidation resistance, machining performance and adaptive behavior under extreme tribological conditions," Materials Today Communications, **31**, 103373 (2022). https://doi.org/10.1016/j.mtcomm.2022.103373
[22] S. Siwawut, C. Saikaew, A. Wisitsoraat, and S. Surinphong, "Cutting performances and wear characteristics of WC inserts coated with TiAlSiN and CrTiAlSiN by filtered cathodic arc in dry face milling of cast iron," Int. J. Adv. Manuf. Technol. **97**, 3883–3892 (2018). https://doi.org/10.1007/s00170-018-2200-x
[23] W. Lu, G. Li, Y. Zhou, S. Liu, K. Wang, and Q. Wang, "Effect of high hardness and adhesion of gradient TiAlSiN coating on cutting performance of titanium alloy," J. Alloys Compounds, **820**, 153137 (2020). https://doi.org/10.1016/j.jallcom.2019.153137
[24] M. Mikula, D. Plašienka, D.G. Sangiovanni, M. Sahul, T. Roch, M. Truchlý, M. Gregor, et al., "Toughness enhancement in highly NbN-alloyed Ti-Al-N hard coatings," Acta Mater. **121**, 59–67 (2016) https://doi.org/10.1016/j.actamat.2016.08.084
[25] S.A. Glatz, R. Hollerweger, P. Polcik, R. Rachbauer, J. Paulitsch, and P.H. Mayrhofer, "Thermal stability and mechanical properties of arc evaporated Ti-Al-Zr-N hard coatings," Surf. Coat. Technol. **266**, 1–9 (2015). https://doi.org/10.1016/j.surfcoat.2015.01.042
[26] K. Yang, G. Xian, H. Zhao, H. Fan, J. Wang, H. Wang, and H. Du, "Effect of Mo content on the structure and mechanical properties of TiAlMoN films deposited on WC–Co cemented carbide substrate by magnetron sputtering," Int. J. Refract. Met. Hard Mater. **52**, 29–35 (2015). https://doi.org/10.1016/j.ijrmhm.2015.04.016
[27] L. Tomaszewski, W. Gukbinski, A. Urbanowicz, T. Suszko, A. Lewandowski, and W. Gulbinski, "TiAlN based wear resistant coatings modified by molybdenum addition," Vacuum, **121**, 223–229 (2015). https://doi.org/10.1016/j.vacuum.2015.08.027
[28] S.A. Glatz, H. Bolvardi, S. Kolozsvári, C.M. Koller, H. Riedl, and P.H. Mayrhofer, "Arc evaporated W-alloyed Ti-Al-N coatings for improved thermal stability, mechanical, and tribological properties," Surf. Coatings Technol. **332**, 275-282 (2017). https://doi.org/10.1016/j.surfcoat.2017.05.097
[29] J. Mo, Z. Wu, Y. Yao, Q. Zhang, and Q. Wang, "Influence of Y-Addition and Multilayer Modulation on Microstructure, Oxidation Resistance and Corrosion Behavior of $Al_{0.67}Ti_{0.33}N$ Coatings," Surf. Coat. Technol. **342**, 129–136 (2018). https://doi.org/10.1016/j.surfcoat.2018.02.071
[30] M. Moser, P.H. Mayrhofer, L. Székely, G. Sáfrán, and P.B. Barna, "Influence of bipolar pulsed DC magnetron sputtering on elemental composition and micro-structure of Ti–Al–Y–N thin films," Surface and Coatings Technology, **203**(1–2), 148-155 (2008). https://doi.org/10.1016/j.surfcoat.2008.08.042
[31] L. Székely, G. Sáfrán, V. Kis, Z.E. Horváth, P.H. Mayrhofer, M. Moser, G. Radnóczi, et al., "Crossover of texture and morphology in $(Ti_{1-x}Al_x)_{1-y}Y_yN$ alloy films and the pathway of structure evolution," Surface and Coatings Technology, **257**, 3-14 (2014). https://doi.org/10.1016/j.surfcoat.2014.08.071
[32] R. Rachbauer, D. Holec, M. Lattemann, L. Hultman, and P.H. Mayrhofer, "Electronic origin of structure and mechanical properties in Y and Nb alloyed Ti-Al-N thin films," Int. J. Mater. Res. **102**, 735–742 (2011). https://doi.org/10.3139/146.110520
[33] R. Aninat, N. Valle, J.-B. Chemin, D. Duday, C. Michotte, M. Penoy, L. Bourgeois, and P. Choquet, "Addition of Ta and Y in a Hard Ti-Al-N PVD Coating: Individual and Conjugated Effect on the Oxidation and Wear Properties," Corros. Sci. **156**, 171-180 (2019). https://doi.org/10.1016/j.corsci.2019.04.042

[34] M. Moser, D. Kiener, C. Scheu, and P.H. Mayrhofer, "Influence of Yttrium on the Thermal Stability of Ti-Al-N Thin Films," Materials, **3**, 1573–1592 (2010). https://doi.org/10.3390/ma3031573
[35] L.A. Donohue, D.B. Lewis, W.D. Münz, M.M. Stack, S.B. Lyon, H.W. Wang, and D. Rafaja, "The influence of low concentrations of chromium and yttrium on the oxidation behaviour, residual stress and corrosion performance of TiAlN hard coatings on steel substrates," Vacuum, **55**, 109–114 (1999). https://doi.org/10.1016/S0042-207X(99)00135-9
[36] H. Tawancy, N. Abbas, and A. Bennett, "Role of Y during high temperature oxidation of an M-Cr-Al-Y coating on an Ni-base superalloy," Surf. Coat. Technol. **68–69**, 10–16 (1994). https://doi.org/10.1016/0257-8972(94)90130-9
[37] S. Wang, Y. Kong, L. Chen, and Y. Du, "Adsorption behavior of oxygen on Ti0.5Al0.5N (001) surface with X-doped (X = La, Ce, Y, Hf, Zr, Ta, Cr, Si): A first-principles study," Applied Surface Science, **639**, 158245 (2023). https://doi.org/10.1016/j.apsusc.2023.158245
[38] R. Hollerweger, H. Riedl, M. Arndt, S. Kolozsvari, S. Primig, and P.H. Mayrhofer, "Guidelines for increasing the oxidation resistance of Ti-Al-N based coatings," Thin Solid Films, **688**, 137290 (2019). https://doi.org/10.1016/j.tsf.2019.05.009
[39] T.C. Rojas, S. Domínguez-Meister, M. Brizuela, and J.C. Sanchez-Lopez, "Influence of Al and Y content on the oxidation resistance of CrAlYN protective coatings for high temperature applications: New insights about the Y role," Journal of Alloys and Compounds, **773**, 1172-1181 (2019). https://doi.org/10.1016/j.jallcom.2018.09.28
[40] L.F. He, J. Shirahata, T. Nakayama, T. Suzuki, H. Suematsu, I. Ihara, Y.W. Bao, et al., "Mechanical properties of $Y_2Ti_2O_7$," Scripta Materialia, **64**(6), 548-551 (2011). https://doi.org/10.1016/j.scriptamat.2010.11.042
[41] Z.B. Qi, Z.T. Wu, and Z.C. Wang, "Improved hardness and oxidation resistance for CrAlN hard coatings with Y addition by magnetron co-sputtering," Surf. Coat. Technol. **259**, 146–151 (2014). https://doi.org/10.1016/j.surfcoat.2014.02.034
[42] K. Zhang, J. Deng, X. Guo, L. Sun, and S. Lei, "Study on the adhesion and tribological behavior of PVD TiAlN coatings with a multi-scale textured substrate surface," Int. J. Refract. Met. Hard Mater. **72**, 292–305 (2018). https://doi.org/10.1016/j.ijrmhm.2018.01.003
[43] P.Eh. Hovsepian, D.B. Lewis, Q. Luo, W.-D. Münz, P.H. Mayrhofer, C. Mitterer, Z. Zhou, and W.M. Rainforth, "TiAlN based nanoscale multilayer coatings designed to adapt their tribological properties at elevated temperatures," Thin Solid Films, **485**, 160 (2005). https://doi.org/10.1016/j.tsf.2005.03.048
[44] S. PalDey, and S.C. Deevi, "Single layer and multilayer wear resistant coatings of (Ti,Al)N: a review," Mater. Sci. Eng. A, **342**(1-2), 58–79 (2003). https://doi.org/10.1016/S0921-5093(02)00259-9
[45] A. Raveh, I. Zukerman, R. Shneck, R. Avni, and I. Fried, "Thermal stability of nanostructured superhard coatings: A review," Surf. Coat. Technol. **201**(13), 6136–6142 (2007). https://doi.org/10.1016/j.surfcoat.2006.08.131
[46] L. Zhu, Y. Zhang, W. Ni, and Y. Liu, "The effect of yttrium on cathodic arc evaporated $Ti_{0.45}Al_{0.55}N$ coating," Surface and Coatings Technology, **214**, 53–58 (2013). http://dx.doi.org/10.1016/j.surfcoat.2012.10.074
[47] A. Hemmati, M. Abdoos, and S.C. Veldhuis, "Developing Ti-Al-Ta-N based coatings: Thermal stability, oxidation resistance, machining performance and adaptive behavior under extreme tribological conditions," Materials Today Communications, **31**, 103373 (2022). https://doi.org/10.1016/j.mtcomm.2022.103373
[48] C. Leyens, M. Peters, P.Eh. Hovsepian, D.B. Lewis, Q. Luo, and W.-D. Münz, "Novel coating systems produced by the combined cathodic arc/unbalanced magnetron sputtering for environmental protection of titanium alloys," Surf. Coat. Technol. **155**, 103–111 (2002). https://doi.org/10.1016/S0257-8972(02)00063-4
[49] M.I. Lembke, D.B. Lewis, W.-D. Münz, and J.M. Titchmarsh, "Significance of Y and Cr in TiAlN Hard Coatings for Dry High Speed Cutting," Surf. Eng. **17**, 153–158 (2001). https://doi.org/10.1179/026708401101517656

НАСЛІДКИ ПРИСУТНОСТІ Y ЯК РЕАКЦІЙНОЗДАТНОГО ЕЛЕМЕНТА В КАТОДНО-ДУГОВОМУ ЗАХИСНОМУ ПОКРИТТІ TiAlN ДЛЯ ТРИБОЛОГІЧНИХ ЗАСТОСУВАНЬ

Ольга Максакова[a,b], Вячеслав Береснєв[a], Сергій Литовченко[a], Марія Чапловичова[b], Любомир Чаплович[b], Мартін Куси[b], Іріна Дощечкина[c]

[a]Харківський національний університет імені В.Н. Каразіна, Харків, м. Свободи, 4, 61022, Україна
[b]Інститут матеріалознавства, Словацький технологічний університет у Братиславі, 25, вул. Яна Ботту, 917 24, Трнава, Словаччина
[c]Харківський національний автомобільно-дорожній університет, вул. Я. Мудрого, 61200, м. Харків, Україна

Приведено результати досліджень впливу Y як реакційноздатного елемента на властивості покриттів TiAlN отриманих методом вакуумно-дугового осадження. Зміни в структурі та властивостях були проаналізовані за допомогою SEM у поєднанні з EDX, XRD, аналізом вдавлення та аналізом зносу. Показано присутності Y змінює кристалічну фазу покриття $Ti_{0,6}Al_{0,34}Y_{0,06}N$. Він складається з комбінації кубічної структури типу NaCl (базова фаза) і структури вюрциту (додаткова фаза). Крім того, це призводить до дрібного розміру зерна (12 нм) і нано-стовпчастої структури. Висока твердість частково є результатом твердіння розчину через включення більших атомів Y у решітку TiAlN у місцях розташування атомів металу. Зменшений розмір зерна 12 нм також сприяє підвищенню твердості покриття. Твердість становить 31±2,5 ГПа, модуль пружності 394,8±35,8 ГПа. Залишкове напруження приблизно в три рази (−3352±64 МПа) перевищує покриття TiAlN (−720 МПа). Крім того, високий рівень стискаючої напруги сприяє підвищенню твердості, оскільки дефекти, відповідальні за власну стискаючу напругу, є перешкодою для руху дислокації. Покращену твердість експериментального покриття можна пояснити потрійним ефектом: зміцнення розчину, подрібнення зерна та високе залишкове напруження стиску. Додавання Y свідчить про сповільнене зростання оксидного шару на поверхні покриття під час випробування на знос. Після додавання Y іони Y переважно відокремлюються на границях зерен, і тому ефективно затримують дифузію кисню всередину. Додавання Y сприяє утворенню щільного Al_2O_3, який є ефективним у стримуванні дифузії і, отже, захищає покриття від окисного зношування.

Ключові слова: *вакуумно-дугове осадження; покриття; вюрцитна фаза; твердість; знос; критичні навантаження*